Soft Matter

PAPER

View Article Online
View Journal | View Issue

Cite this: *Soft Matter*, 2016, 12, 9657

Dynamic self-organization of side-propelling colloidal rods: experiments and simulations†

Hanumantha Rao Vutukuri,*[a] Zdeněk Preisler,[b] Thijs H. Besseling,[b] Alfons van Blaaderen,[b] Marjolein Dijkstra*[b] and Wilhelm T. S. Huck*[a]

Received 31st July 2016,
Accepted 14th November 2016

DOI: 10.1039/c6sm01760f

www.rsc.org/softmatter

In recent years, there is a growing interest in designing artificial analogues of living systems, fueled not only by potential applications as 'smart micro-machines', but also by the demand for simple models that can be used to study the behavior of their more complex natural counterparts. Here, we present a facile, internally driven, experimental system comprised of fluorescently labeled colloidal silica rods of which the self-propulsion is powered by the decomposition of H_2O_2 catalyzed by a length-wise half Pt coating of the particles in order to study how shape anisotropy and swimming direction affect the collective behavior. We investigated the emerging structures and their time evolution for various particle concentrations in (quasi-)two dimensional systems for three aspect ratios of the rods on a single particle level using a combination of experiments and simulations. We found that the dynamic self-organization relied on a competition between self-propulsion and phoretic attractions induced by phoresis of the rods. We observed that the particle clustering behavior depends on the concentration as well as the aspect ratio of the rods. Our findings provide a more detailed understanding of dynamic self-organization of anisotropic particles and the role the propulsion direction plays in internally driven systems.

Introduction

Colloids have been successfully used as condensed matter model systems for studying fundamental aspects of both equilibrium, as well as non-equilibrium phase behaviour.[1–7] Non-equilibrium systems exhibit a rich collective behaviour such as clustering, segregation, and anomalous density fluctuations.[8–11] Understanding and controlling such collective phenomena is a major challenge and is relevant across many disciplines, ranging from microbiology and biophysics to chemical technology and biotechnology.[12–14] Many systems with such behaviour can be found in nature, for instance, schools of fish,[15] flocks of birds,[16] and colonies of bacteria.[17,18] On the other hand, recent progress in the synthesis of ever more complex model systems has made it possible to fabricate a wide variety of self-propelled particles, including Janus spheres,[19,20] bimetallic rods,[21] bimetallic Janus nanofibers,[22] stomatocytes,[23] multilayer metallic microtubules,[24] rollers,[25] and active granular particles,[26,27] based on different self-propulsion mechanisms (for a more complete list, see *e.g.* the review papers[8–11,14]). In particular, micron-sized self-propelled (active) particle systems have attracted a considerable interest as they offer the possibility to study dynamics and structure quantitatively in dense suspensions on a single particle level. In contrast to passive particles that are in thermodynamic equilibrium with the solvent they are dispersed in, active particles are internally driven far from equilibrium by converting energy from their local environment into active motion. In the case of self-propelled spherical particles, clustering and living crystals have been reported.[8–10,28] Furthermore, on comparable length and time scales, motile microorganisms like many bacteria, self-organize into remarkable macroscopic patterns by collective dynamics, ranging from swarms to active turbulence.[17,18,29] Several recent experiments, simulations and theoretical studies have predicted that not only particle shape[30–32] and the system composition,[33,34] but also swimming speed and swimming direction[18,35] play crucial roles in the collective behaviour of active systems. For instance, swarming motion, jamming, and active turbulence were predicted in the case of rod-like active particle systems,[36] but experimental realizations of those phases with synthetic anisotropic microswimmers scarcely exist. We believe that an active rod-like particle might be the closest shape to mimic some of the natural bacterial systems such as the *E. coli* bacterium.[17,18] To date, experiments on bimetallic rods, *i.e.* Au–Pt rods, have only been reported at dilute concentrations.[21,37,38] This can be attributed to the fact that these fully metallic particles strongly absorb and scatter light that precludes the study of concentrated dispersions even in 2D

[a] *Institute for Molecules and Materials, Radboud University, 6525 AJ, Nijmegen, The Netherlands. E-mail: hanumantharaov@gmail.com, W.Huck@science.ru.nl*
[b] *Soft Condensed Matter, Debye Institute for Nanomaterials Science, Utrecht University, 3584 CH, The Netherlands. E-mail: m.dijkstra@uu.nl*

† Electronic supplementary information (ESI) available: We included our simulation model and 13 supporting figures with captions. In addition, we added 3 supporting movies (in avi format). See DOI: 10.1039/c6sm01760f

or quasi-2D systems.[12–14,21,39,40] To the best of our knowledge, a study on the collective behaviour of synthetic rod-like swimmers on a colloidal scale has not been reported. Here, we study the dynamic self-organization of fluorescently labelled side-propelling colloidal rods in dense suspensions on a single particle level in quasi-2D systems. We refer to our system as quasi-2D as the gravitational length of the rods was estimated to range from 100 nm to 400 nm, which is comparable with the diameter of the rods. The gravitational length corresponds to the height difference for which the change in gravitational energy of a rod equals the thermal energy k_BT. Despite this, we occasionally observed rods that moved out of the plane from the lower glass plate, which happened mostly at low concentrations due to the self-propulsion. In addition, we performed simulations using a minimal 2D model of this system. We investigate, both in experiments and simulations, the effect of the swimming direction together with the shape anisotropy on the collective behaviour of side-propelled rods as a function of concentration, aspect ratio, and activity.

Results and discussion

Our experimental system consists of half-side platinum-coated silica rods, *i.e.* Janus rods, which are fluorescently labelled. We coated the particles along the major axis as can be seen in the bottom-inset of Fig. 1a. These particles diffused isotropically by thermal fluctuations, when suspended in water. However, these

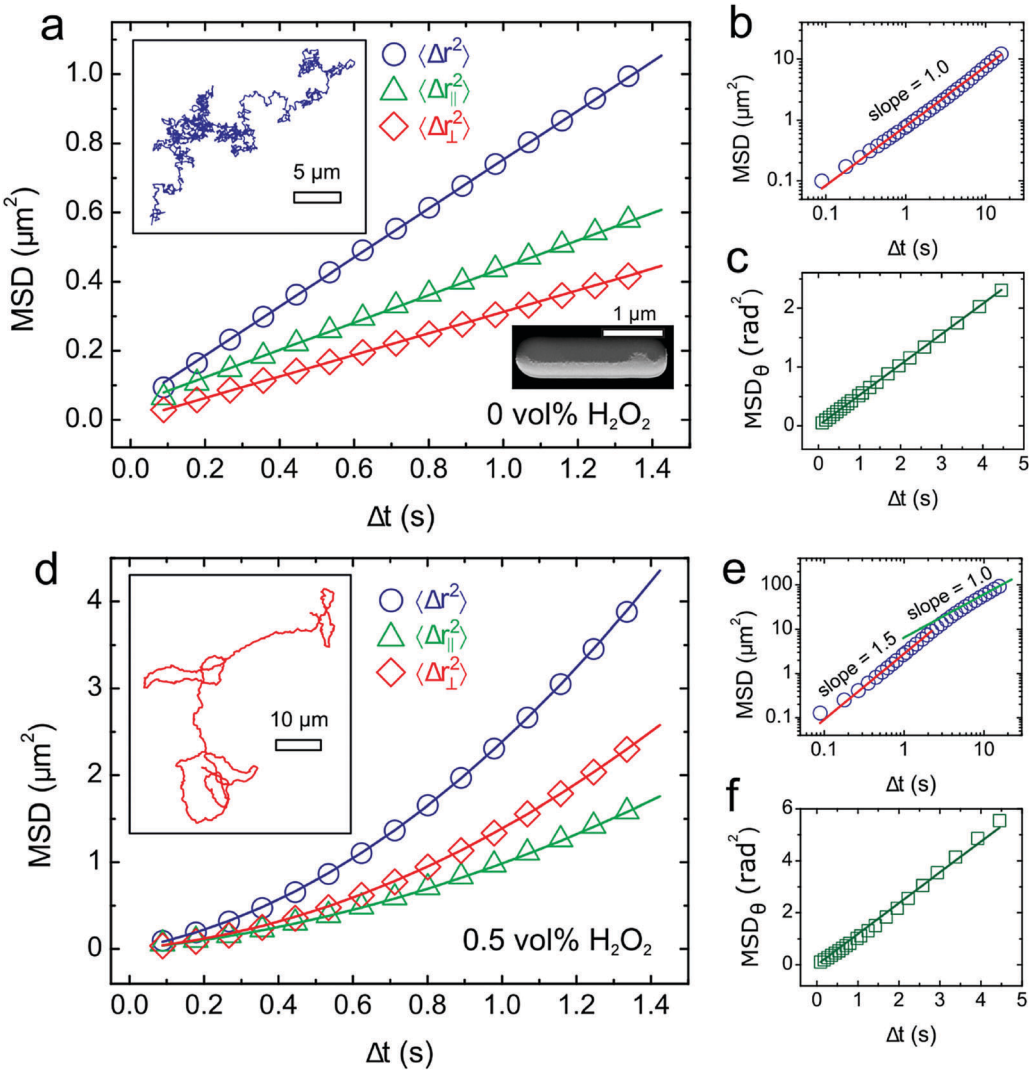

Fig. 1 Mean square and mean square angular displacements of passive (a–c), and active rods in 0.5 vol% H_2O_2 solution (d–f). (a and d) Short-time translational MSDs. The blue circles are the rotationally averaged and total MSD $\langle \Delta r^2(\Delta t) \rangle$, the green triangles are $\langle \Delta r_{\parallel}{}^2(\Delta t) \rangle$ along the long axis, and the red diamonds are $\langle \Delta r_{\perp}{}^2(\Delta t) \rangle$ along the short axes of the particles. The solid lines denote the fits as obtained from the MSD equations (see ESI†). Top-left insets illustrate typical trajectories of passive and active rods, respectively. Bottom-right inset shows a scanning transmission electron microscopy (STEM) image of a Janus rod. (b) Passive rods show the normal diffusive behavior. (e) Active rods show super diffusive behavior at short times, whereas diffusive-like behavior is seen at long times. (c and f) Angular MSD_θ of rods. The green squares are experimental measurements. The solid lines denote fits following the mean square angular displacements (MSAD) equations (see ESI†).

rods can be made self-propelling upon the addition of hydrogen peroxide (H_2O_2), which enables a catalytic reaction. The platinum-catalyzed decomposition reaction of H_2O_2 generates a concentration gradient of ions across the surface of the particles, inducing the self-propulsion perpendicular to the long axis in the direction of the non-coated surface. Although the underlying mechanism responsible for the propulsion is still debated,[41] the propulsion mechanism is most likely determined by a combination of diffusiophoresis and self-electrophoresis.[19,42,43] To prevent the unwanted formation of O_2 bubbles we performed our experiments at low fuel concentration (0.5 vol% H_2O_2) at which, single rods of aspect ratio, a = 4.1, were propelled with a speed of 1.0 μm s^{-1} (see ESI†). We measured the translational mean square displacements (MSD) along the major and minor axes of rods as well as the mean square angular displacement (MSD_θ) from the particle coordinates and orientations as obtained from the image analysis using the particle-tracking algorithms as described in ref. 44. We found that the short-time MSDs were significantly different from their equilibrium counter parts as shown in Fig. 1a and d. In addition, the self-propelled particles showed a crossover from super-diffusive to diffusive behavior (Fig. 1e), and we determined the translational and the rotational diffusion coefficients from fitting the MSDs and MSD_θ, respectively. Note that we extended previous models[11,45] on active diffusion of self-propelled spherical particles to our active rods by taking into account the shape anisotropy (see ESI†). We observed an enhancement in the transverse and parallel translational diffusion constants ($D_{prop,\perp}$ = 1.29 μm^2 s^{-1}, $D_{prop,\parallel}$ = 0.77 μm^2 s^{-1}) of the active rods with respect to passive dispersions of the same rods ($D_{eq,\perp}$ = 0.16 μm^2 s^{-1}, $D_{eq,\parallel}$ = 0.20 μm^2 s^{-1}). The enhanced diffusivity can be explained by the fact that the particles performed a persistent random walk.[8,12,21,28,46] We also observed an enhancement in the rotational diffusion coefficient of the active particles ($D_{prop,\theta} \approx$ 0.59 rad^2 s^{-1}) with respect to the same passive rods ($D_{eq,\theta} \approx$ 0.26 rad^2 s^{-1}), see Fig. 1c and e. We note that for very long passive rods the ratio between the parallel to perpendicular diffusion coefficients is equal to 2, while this ratio is less than 2 for finite size rods.[47,48] Tirado *et al.* included the finite size effects and derived explicit expressions[48] for the parallel and perpendicular diffusion coefficients as a function of aspect ratio (see ESI†). For a comparison, we estimated the theoretical values of the translational diffusion coefficients for passive rods (a = 4.1) to be $D_\parallel$ = 0.36 μm^2 s^{-1}, $D_\perp$ = 0.29 μm^2 s^{-1}. The ratio between the parallel and perpendicular diffusion coefficients is 1.24. The experimentally measured values are $D_\parallel$ = 0.20 μm^2 s^{-1}, $D_\perp$ = 0.16 μm^2 s^{-1} and the ratio is 1.25. We believe that the discrepancy between the experimental and theoretical values might come from the hydrodynamic interaction between the wall and the rod. The calculation of full hydrodynamic rod-wall interactions is very challenging and beyond the scope of the present study.

Next, we investigated the dynamic self-organization and state behaviour at different particle concentrations, both experimentally and by means of computer simulations. We chosen the range of particle concentration in such a way that we can capture the concentration dependent clustering behavior of side-propelling rods. We first discuss the structural evolution of clustering (see Fig. 2) as observed in experiments at a surface area fraction, $\varphi_s = Na_p/A \approx 0.07$ with N the number of particles, A the surface area of the system, and a_p the surface area of a particle. When a single self-propelled rod with aspect ratio, l/d = 4.1 (l denotes the end-to-end length of the rod and d the diameter.), encountered another rod moving in the opposite direction, they tend to form a doublet (pair) in a side-by-side fashion as shown in Fig. 2b. We occasionally observed a single particle moving in or out of the 2D plane. This can be attributed to fact that the gravitational length ($\approx$390 nm) is comparable to the particle thickness. Alternatively, this can also result from a change in the propulsion direction, however, once clusters were formed we did not observe this behaviour. The two opposing propulsion forces of the particles in a doublet effectively balance each other resulting in much smaller diffusion of the doublet with respect to the single rods. However, due to Brownian forces the relative positions of the rods can alter, giving rise to an instantaneous net force, and consequently in linear and circular motions. We note that this behaviour is different from that observed in systems of active spheres and tip-propelled rods.[9,49] It demonstrates that the collective behaviour does not depend only on the particle shape but also strongly depends on the particle propulsion direction. When a third rod joins a doublet then the whole cluster experiences a net force, and the triplet immediately starts to move either in a linear or in a circular fashion. These triplets subsequently self-organize into tetramers, where the fourth rod can join either along or perpendicular to the major axis of the triplet (Fig. 2d).

As the dynamic clustering continues, the tetramers further organize themselves into multimers, eventually forming larger clusters depending on the particle concentration. The whole assembly process is dynamic so the small clusters split or grow by joining new particles or by merging smaller clusters together. Fig. 2 and Movie S1 (ESI†) demonstrate the temporal evolution of the side-propelling rods.

To shed light on how the state behaviour depends on the rod density, we varied the particle concentration while keeping the fuel concentration constant as shown in Fig. 3. At a dilute particle concentration, $\varphi_s \approx 0.01$, predominantly doublets and triplets were observed (Fig. 3a). In addition to these structures, rods organized into tetramers and small clusters at a particle concentration, $\varphi_s \approx 0.07$ (Fig. 3c). At concentration $\varphi_s \approx 0.26$, we observed a phase consisting of active clusters (Fig. 3e). Although the system is dynamic and the clusters are changing rapidly with time, on average clusters do not grow, however, they are constantly splitting and merging over time suggesting that this system was observed in a dynamic steady-state. Further, we varied the particle's aspect ratio (l/d) to investigate how it affects the dynamic self-organization. Due to experimental limitations it is challenging to study a whole range of aspect ratios. Nevertheless, we studied the collective behaviour for two more aspect ratios, namely l/d = 7.0, and 20.4. We did not observe any qualitative difference in the behavior for aspect ratios l/d = 4.1, and 7.0 (see Fig. 3 and Fig. S1, ESI†). Moreover, we observed similar trends in the clustering behaviour even

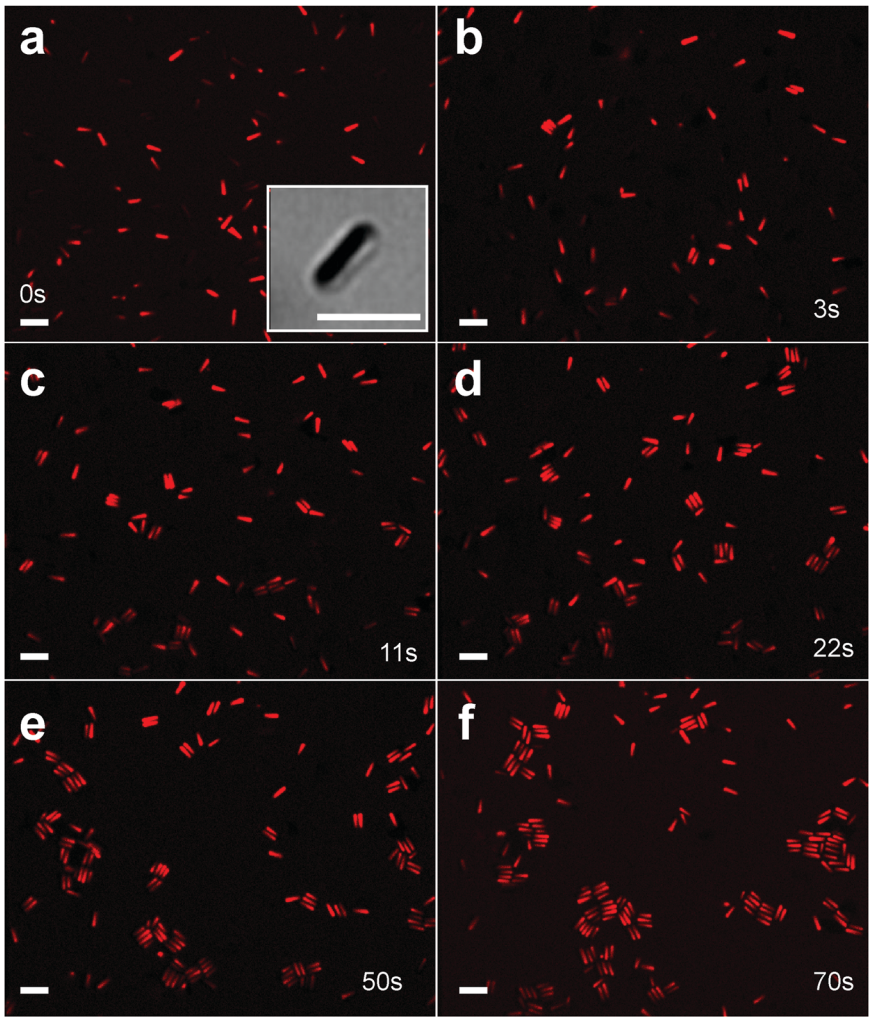

Fig. 2 Time-lapse structural evolution of active rods. (a–f) Confocal micrographs of Janus rods with aspect ratio l/d = 4.1 reveal the structural evolution of self-propelled Janus rods at a fuel concentration of 0.5 vol% H_2O_2. Inset depicts the bright field image of a Pt coated (dark side) silica rod. The scale bar is 5.0 μm and the inset scale bar is 3.0 μm.

with binary mixtures of rods with aspect ratios 4.1 and 7.0 as shown in Fig. S2 (ESI†). While the rods with aspect ratio l/d = 20.4 formed doublets, triplets, and tetramers at dilute concentrations (Fig. S3a, ESI†), they got jammed at higher particle concentrations ($\varphi_s \approx 0.09$) as shown in Fig. S3b (ESI†).

After increasing the particle activity by adding a high fuel concentration (2.0 vol% H_2O_2) and at this fuel concentration rods were propelled with a speed of 1.6 μm s^{-1}. For the particle concentration of $\varphi_s \approx 0.28$, we first observed small clusters of rods (l/d = 4.1) being formed, which then evolved into a few bigger clusters by merging of smaller ones within a time span of 10–15 min (Fig. S4, ESI†). At this point, we did not observe any further merging of the clusters in time, which might be caused by slow dynamics of the big clusters, together with the limited availability of fuel necessary for the propulsion. We assume that the final state could, in principle, be the condensation of particles into a single cluster. We note that, the system resembles phase separation between dense "living" clusters and a dilute gas (Fig. 4). Fig. 4b reveals the internal structure of such a cluster. However, the internal structure of such a big cluster did not change with time suggesting that the system is in a dynamically trapped state. In order to quantify the ordering we introduced a local order parameter. We evaluated the probability distribution function (PDF) of the dot product between the orientation vectors of two rods, which are separated by a distance, r, smaller than a cut-off distance σ_{cut}. We did not observe any long-range positional and orientational ordering within a big cluster, but a local orientational ordering of rods within clusters (Fig. 4c) has been observed. We note the rods are predominately ordered parallel to each other in all cases.

Dynamic clustering and phase separation in active systems can be divided into two categories: (i) purely motility induced phase separation,[20,50–52] and (ii) a combination of motility and short-range attractions[53–56] induced phase separation. Several simulation and theoretical studies have predicted that motility alone is sufficient to induce clustering, and phase separation of active systems due to reduced motility at sufficiently high densities.[50,52,57] On the other hand, most of the experimental

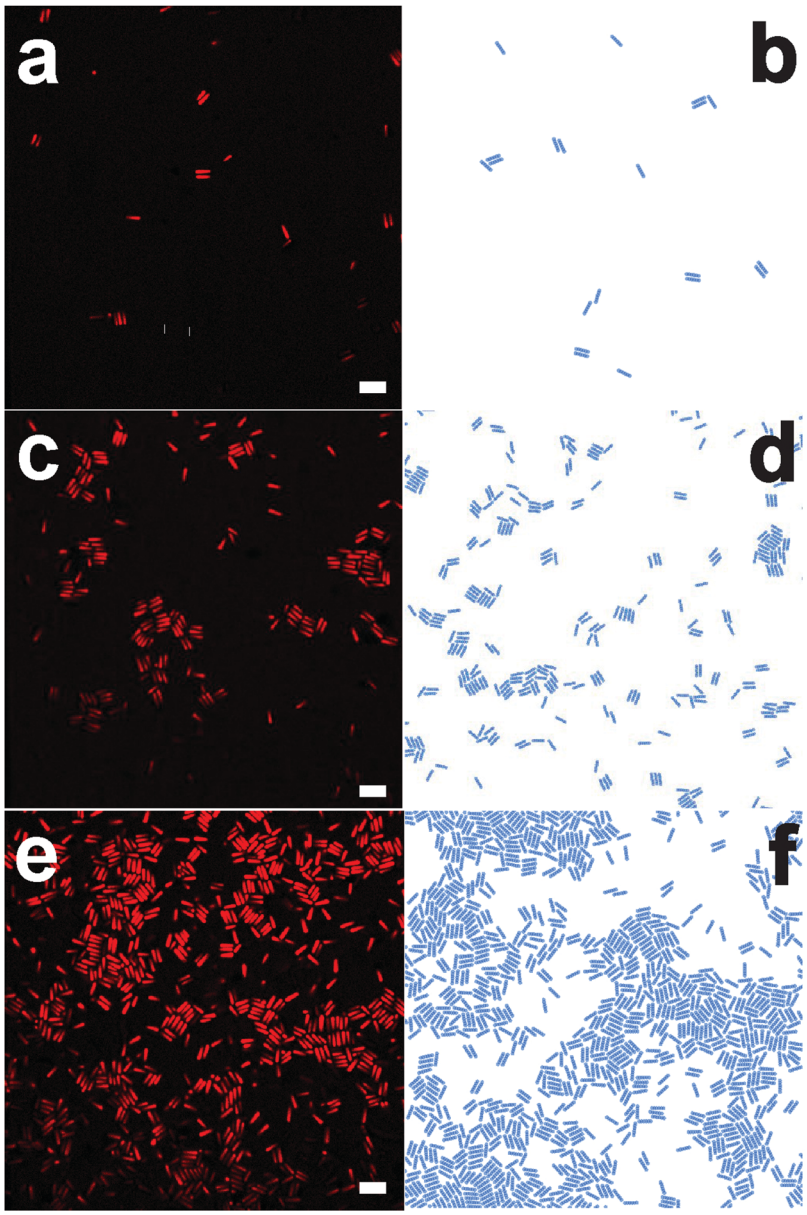

Fig. 3 Experimental and simulation results on the dynamic self-organization of Janus rods with aspect ratio l/d = 4.1 as a function of particle concentration φ_s at a fuel concentration of 0.5 vol% H_2O_2. (a) Mainly doublets, occasionally triplets at very dilute particle concentration, $\varphi_s \approx 0.01$. (c) Small clusters of active rods at particle concentration, $\varphi_s \approx 0.07$. (e) Big clusters of rods at moderate particle concentration $\varphi_s \approx 0.26$. (b, d and f) Typical configurations from the simulations for the corresponding concentrations. The parameters used: (b) activity F_a = 2.0, and attraction strengths $\beta\lambda_1$ = 2.0, (d) F_a = 2.0, and $\beta\lambda_1$ = 2.0, and (f) F_a = 1.8, and $\beta\lambda_1$ = 1.0 (see ESI†). The scale bar is 5.0 μm.

systems consisting of micron-sized catalytically-driven self-propelled particles, *e.g.* Janus particles in H_2O_2, almost always experience a net attraction[19,28,41] due to the nonuniformity in the chemical fuel concentration between the particles. In order to mimic the experientially observed dynamic clustering and phase separation in self-propelled particle systems, several simulation studies have included short-ranged attractions[54–56] to the motility and are able to predict the experimentally observed dynamic clustering and phase separation. More recently, Tung *et al.* have implemented this concept to anisotropic (*i.e.* dumbbell-shaped) particles and predicted a rich behavior such as rotating clusters, living clusters, and living stripes.[58] We believe that our experimental system fall into the second category, *i.e.* a combination of motility and attractions induced dynamic clustering and phase separation.

For rods with aspect ratio l/d = 7.0 and the same fuel concentration (2.0 vol%), we did not observe the formation of big clusters as we found for the shorter rods. We note that we were not able to further increase the particle's activity because we were already close to the hydrogen peroxide concentration (>2.0 vol%) where bubble formation occurs that precluded studies at higher levels of activity.

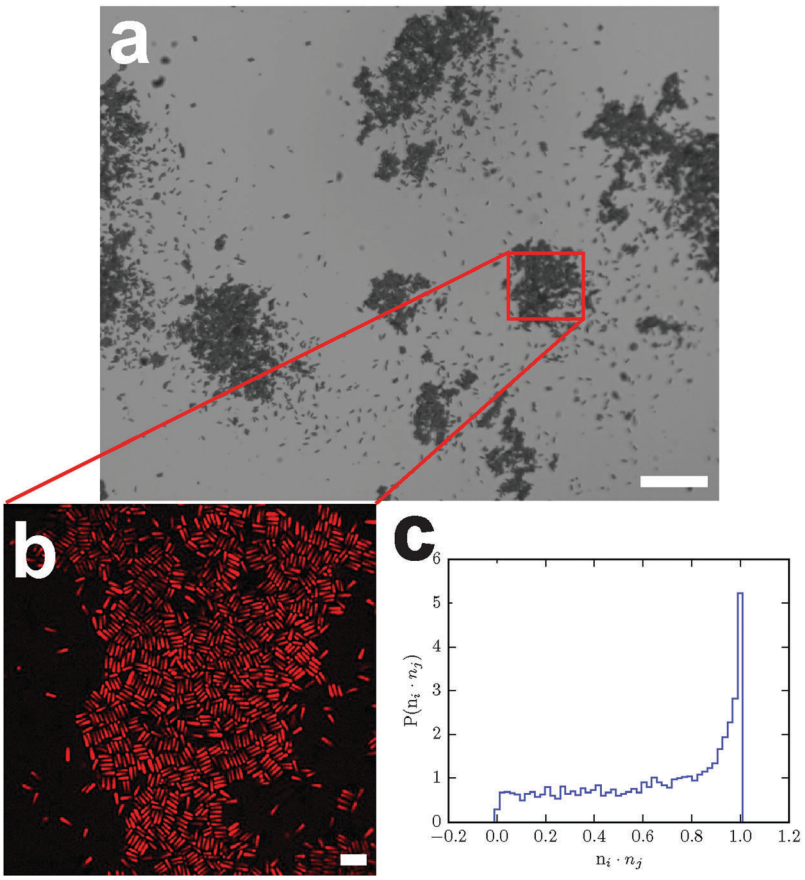

Fig. 4 Self-organization at fuel concentration 2.0 vol% and particle concentration of $\varphi_s \approx 0.28$. (a) Bright field image shows the phase separation. (b) Confocal image of a single giant cluster as depicted by the red box in figure (a). (c) The orientation probability distribution function $P(n_i \cdot n_j)$ with n_i the orientation vector of particle i. The scale bars are 70.0 μm and 5.0 μm, respectively.

We note that we observed attractions, in particular, between the tips of the rods in the presence of the fuel as shown in Fig. 5. This is quite evident from Movie S2 (ESI†), where the two actively moving doublets attracted each other and organized into staggered configuration in a linear direction that immediately starts rotating. We observed that this configuration is rather dynamic as it can easily split or join with other particles or doublets indicating that the attraction between these pairs is weak. Although we do not know the exact origin of the attraction, we speculate that it might be of phoretic origin. We did not observe any sign of attractions between the rods in the absence of the fuel. In order to further confirm the attractions between the active rods, we applied an external AC electric field to the active particle clusters. At low field strength (E_{rms} = 0.001 V μm^{-1}, f = 500 kHz) the whole cluster aligned in the field direction, suggesting that the attractions between the particles overcome the induced dipolar attractions between the particles (Fig. S5b, ESI†). When we further increased the field strength the induced dipolar interactions (E_{rms} = 0.01 V μm^{-1}, f = 500 kHz) between the rods overcame the attractions and the whole cluster transformed into zig-zag like configuration (Fig. S5c, ESI†), which is the most energetically favourable configuration for Janus rods interacting solely with induced dipoles.[59–61]

To better understand the experimental state behaviour we complemented our study with computer simulations. We performed overdamped Brownian dynamics simulations of side-propelled rods to investigate the effect of particle shape anisotropy together with the particle propulsion strength and direction. We developed a minimal model that mimics our experimental system of colloidal rods using various assumptions and simplifications. In particular, we assumed that the particles are confined to two dimensions and we neglected the hydrodynamic interactions between the colloidal particles as well as the particle interactions with the walls. Additionally, we assumed that our system is monodisperse and the self-propelling force is constant in time, and we disregarded the axial rotational diffusion, *i.e.*, diffusion around the major-axis. We modelled each colloidal rod by n segments equidistantly aligned on a line,[36] where each segment is described by a pair potential (see ESI†). The total interaction of two rods is the sum of all the segment-segment interactions between the two rods. In attempt to find an appropriate model to obtain quantitative agreement with the experiments, we first performed simulations with purely repulsive self-propelled rods. We observed experimentally as well as in our computer simulations that, in the case of side-propelled rods, the rod-doublet configuration is stable (Fig. 3a and b). We explain this by the fact that the torque

generated due to the long edges (with which the two rods touch) suppresses the effect of the rotational diffusion, which is responsible for the break-up of a particle pair. However, we were not able to reproduce our experimentally observed state behaviour as a function of particle concentration when the rods are interacting solely *via* a pure repulsive potential in simulations. Moreover, large clusters were observed in experiments suggesting that the formation of large clusters is not only activity driven but is also attraction induced. Based on our experimental observations (Fig. 5) we included the attractions between segments belonging to different rods in our simulations. The attractions observed in the experiments appeared to be anisotropic. In particular, we observed a stronger attraction between the tips of the rods. We included this behaviour in our model by changing the attractive interactions between the end segments only after which we recovered a qualitative agreement with the experiments (for more details see ESI†). Movie S3 (ESI†) demonstrates the clustering behaviour of side-propelling rods with and without added attractions for a fixed activity of rods. To find the optimum conditions we simulate the state behaviour of side-propelled rods for a wide range of propulsion strengths or activities (F_a), attraction strengths ($\beta\lambda_1$), and number densities (see ESI† and Fig. S8–S12). Simulations closely matching the experimental results are shown in Fig. 3b, d and f. In addition, we find that big clusters as observed in Fig. 4 are only formed at sufficiently high attraction strength and activity. Therefore, we suspect that the experimentally observed phase separation (Fig. 4) of short rods (l/d = 4.1) might be a combination of activity and fuel concentration depended phoretic attractions between the rods. We summarized all our observed phases in a more qualitative manner in the diagram as shown in Fig. S13 (ESI†).

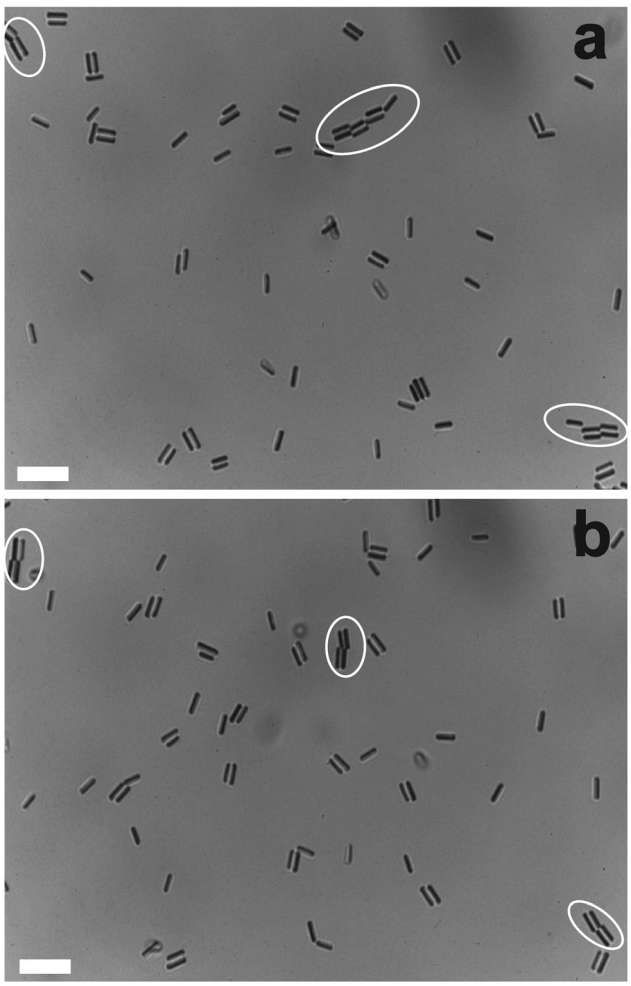

Fig. 5 Doublets and staggered chains of self-propelled rods. Time-lapsed bright field images reveal the staggering configuration of doublets of rods (highlighted by the white ellipsoids) in 0.5 vol% H_2O_2. The time difference between the two images is about 30 s. The scale bar is 5.0 μm.

Conclusions

To summarize, we studied the (quasi-)2D dynamic self-organization of side-propelled rods using fluorescently labelled Janus silica rods with support of computer simulations. Our model system allowed us to follow the dynamics of the self-organization in dense suspensions on a single particle level. In addition, we were able to simultaneously study both the translational and rotational diffusion of the particles and we measured enhanced self-diffusion of the particles consistent with a persistent random walk. We found that dynamic clustering depended on particle concentration, and similar behaviour was observed even for mixtures of rods of different aspect ratios l/d = 4.1, and 7.0. At higher densities and higher activities, we observed a phase consisting of large clusters in coexistence with a dilute gas phase for rods with an aspect ratio of 4.1, which resembled a gas–liquid phase separation. We hypothesize that the experimentally observed phase separation resulted from a combination of self-propulsion and phoretic attractions between the particles. As in our simulations we were not able to reproduce the experimentally observed clustering behaviour and in general the 'state' behaviour unless the specific attractions at the tips of the rods were added into the simulation model. Our study highlights the importance and added possibilities to tune systems by the anisotropy in particle shape and in the self-propulsion direction of anisotropically shaped active particles, features already found often in biological active systems.

Materials and methods

Particle synthesis

Fluorescently labelled silica rods were synthesized following the method of Kuijk *et al.*[62,63] We used three different aspect ratios (l/d) of rods: (i) the small aspect ratio (l/d = 4.1) rods have dimensions of l = 2.6 μm (8.5%), d = 0.63 μm (6.3%), (ii) the aspect ratio l/d = 7 rods have dimensions of l = 4.42 μm (10%), d = 0.63 μm (6%), and (iii) the aspect ratio l/d = 20.4 rods have dimension of l = 10 μm (7%), d = 0.49 μm (6.3%). The shorter rods (l/d = 4.1) that are used in this study were labeled with a gradient in fluorescence level.[62,63]

Janus rods preparation

We first prepared a monolayer of horizontally flat-lying rods by slow drying of rods from a dilute suspension (0.03 vol%) on a clean glass microscope slide. A 15 nm thick layer of platinum (Pt) was then vertically deposited using a sputter coater (Cressington 208HR). Prior to the particle detachment, slides were thoroughly washed with deionized (DI) water, and subsequently the rods were detached by sonicating the slides in DI water for about 10 min. The resulted dispersion was washed and centrifuged 3–4 times with DI water to remove uncoated particles. The surface area fraction (φ_s) was varied by adjusting the concentration of the initial suspension. A typical experiment contained 10 μl of Janus rods into 100 μl solution with a desired fuel concentration.

Sample preparation and particle dynamics

We recorded the particle dynamics using an Olympus IX81 confocal microscope, equipped with an Andor iXon3 camera, Andor 400-series solid-state lasers, a Yokogawa CSU-X1 spinning disk, and a Leica SP8 confocal microscope. Bright-field optical micrographs and videos were recorded using a Nikon microscope equipped with a CCD camera (Olympus CKX41).

Electric field set up

We used a function generator (Agilent, Model 3312 OA) and a wide band voltage amplifier (Krohn-Hite, Model 7602M) to generate the electric fields. The field strength and the frequency were measured using an oscilloscope (Tektronix, Model TDS3052). We constructed an electric cell from a no. 1 glass cover slip (130–160 μm thick, Menzel) onto which two coplanar electrodes were fabricated by sputter coating with 3 nm chromium followed by 20 nm of gold (Cressington 208 h).[64,65] The distance between two gold electrodes was 4 mm (more detail see ESI†).

Particle tracking

We tracked both the positions and orientations of the particles of time-lapsed 2D confocal images by following the method of Besseling *et al.*[44] We then obtained the trajectories of the centre of mass of the rods using the particle tracking programs of Crocker *et al.*[66] To uniquely identify the tip of the (nearly up-down symmetric) rod, it is required that the rotation angle of the individual rods between successive frames is less than $\pi/2$. We kindly refer to the ESI† for the mean square displacement (MSD) and the mean square angular displacement (MSAD) calculations.

Acknowledgements

We thank A. Kuijk for the particle synthesis. W. T. S. H. acknowledges support by a European Research Council Advanced Grant (246812 intercom) and a VICI grant of the Netherlands Organization for Scientific Research. A. v. B. supported by the European Research Council under the European Union's Seventh Framework Programme (FP/2007-2013)/ ERC Grant Agreement no. (291667) HierarSACol. M. D. supported by Stichting voor Fundamenteel Onderzoek der Materie (FOM), which is financially supported by the ''Nederlandse organisatie voor Wetenschappelijke Onderzoek (NWO)''.

References

1 S. C. Glotzer and M. J. Solomon, *Nat. Mater.*, 2007, **6**, 557–562.
2 M. Grzelczak, J. Vermant, E. M. Furst and L. M. Liz-Marzan, *ACS Nano*, 2010, **4**, 3591–3605.
3 S. Sacanna, W. T. M. Irvine, P. M. Chaikin and D. J. Pine, *Nature*, 2010, **464**, 575–578.
4 H. R. Vutukuri, A. F. Demirörs, B. Peng, P. D. J. van Oostrum, A. Imhof and A. van Blaaderen, *Angew. Chem., Int. Ed.*, 2012, **124**, 11411–11415.
5 W. K. Kegel and A. van Blaaderen, *Science*, 2000, **287**, 290–293.
6 F. Li, D. P. Josephson and A. Stein, *Angew. Chem., Int. Ed.*, 2011, **50**, 360–388.
7 H. R. Vutukuri, A. Imhof and A. van Blaaderen, *Angew. Chem., Int. Ed.*, 2014, **53**, 13830–13834.
8 S. A. Igor, *Phys.-Usp.*, 2013, **56**, 79.
9 J. Bialké, T. Speck and H. Löwen, *J. Non-Cryst. Solids*, 2016, **407**, 367–468.
10 M. C. Marchetti, J. F. Joanny, S. Ramaswamy, T. B. Liverpool, J. Prost, M. Rao and R. A. Simha, *Rev. Mod. Phys.*, 2013, **85**, 1143–1189.
11 J. Elgeti, R. G. Winkler and G. Gompper, *Rep. Prog. Phys.*, 2015, **78**, 056601.
12 S. Sengupta, M. E. Ibele and A. Sen, *Angew. Chem., Int. Ed.*, 2012, **51**, 8434–8445.
13 J. Wang and W. Gao, *ACS Nano*, 2012, **6**, 5745–5751.
14 S. Sanchez, L. Soler and J. Katuri, *Angew. Chem., Int. Ed. Engl.*, 2015, **54**, 1414–1444.
15 J. E. Herbert-Read, A. Perna, R. P. Mann, T. M. Schaerf, D. J. T. Sumpter and A. J. W. Ward, *Proc. Natl. Acad. Sci. U. S. A.*, 2011, **108**, 18726–18731.
16 M. Ballerini, N. Calbibbo, R. Candeleir, A. Cavagna, E. Cisbani, I. Giardina, V. Lecomte, A. Orlandi, G. Parisi, A. Procaccini, M. Viale and V. Zdravkovic, *Proc. Natl. Acad. Sci. U. S. A.*, 2008, **105**, 1232–1237.
17 H. C. Berg and D. A. Brown, *Nature*, 1972, **239**, 500–504.
18 H. H. Wensink, J. Dunkel, S. Heidenreich, K. Drescher, R. E. Goldstein, H. Lowen and J. M. Yeomans, *Proc. Natl. Acad. Sci. U. S. A.*, 2012, **109**, 14308–14313.
19 I. Theurkauff, C. Cottin-Bizonne, J. Palacci, C. Ybert and L. Bocquet, *Phys. Rev. Lett.*, 2012, **108**, 268303.
20 I. Buttinoni, J. Bialke, F. Kummel, H. Lowen, C. Bechinger and T. Speck, *Phys. Rev. Lett.*, 2013, **110**, 238301.
21 W. Wang, W. Duan, A. Sen and T. E. Mallouk, *Proc. Natl. Acad. Sci. U. S. A.*, 2013, **110**, 17744–17749.
22 N. K. Reddy, L. Palangetic, L. Stappers, J. Buitenhuis, J. Fransaer and C. Clasen, *J. Mater. Chem. C*, 2013, **1**, 3646–3650.
23 D. A. Wilson, R. J. M. Nolte and J. C. M. van Hest, *Nat. Chem.*, 2012, **4**, 268–274.
24 S. Sanchez, A. A. Solovev, S. M. Harazim and O. G. Schmidt, *J. Am. Chem. Soc.*, 2011, **133**, 701–703.

25 A. Bricard, J. B. Caussin, N. Desreumaux, O. Dauchot and D. Bartolo, *Nature*, 2013, **503**, 95–98.
26 R. F. Ismagilov, A. Schwartz, N. Bowden and G. M. Whitesides, *Angew. Chem., Int. Ed.*, 2002, **41**, 652–654.
27 V. Narayan, S. Ramaswamy and N. Menon, *Science*, 2007, **317**, 105–108.
28 J. Palacci, S. Sacanna, A. P. Steinberg, D. J. Pine and P. M. Chaikin, *Science*, 2013, **339**, 936–940.
29 M. Abkenar, K. Marx, T. Auth and G. Gompper, *Phys. Rev. E: Stat., Nonlinear, Soft Matter Phys.*, 2013, **88**, 062314.
30 R. Di Leonardo, L. Angelani, D. Dell'Arciprete, G. Ruocco, V. Iebba, S. Schippa, M. P. Conte, F. Mecarini, F. De Angelis and E. Di Fabrizio, *Proc. Natl. Acad. Sci. U. S. A.*, 2010, **107**, 9541–9545.
31 B. ten Hagen, F. Kummel, R. Wittkowski, D. Takagi, H. Lowen and C. Bechinger, *Nat. Commun.*, 2014, **5**, 4829.
32 A. Sokolov, M. M. Apodaca, B. A. Grzybowski and I. S. Aranson, *Proc. Natl. Acad. Sci. U. S. A.*, 2010, **107**, 969–974.
33 K. Yeo, E. Lushi and P. M. Vlahovska, *Phys. Rev. Lett.*, 2015, **114**, 188301.
34 J. Stenhammar, R. Wittkowski, D. Marenduzzo and M. E. Cates, *Phys. Rev. Lett.*, 2015, **114**, 018301.
35 N. H. P. Nguyen, D. Klotsa, M. Engel and S. C. Glotzer, *Phys. Rev. Lett.*, 2014, **112**, 075701.
36 H. H. Wensink and H. Lowen, *J. Phys.: Condens. Matter*, 2012, **24**, 464130.
37 Y. Hong, N. M. K. Blackman, N. D. Kopp, A. Sen and D. Velegol, *Phys. Rev. Lett.*, 2007, **99**, 178103.
38 M. S. Davies Wykes, J. Palacci, T. Adachi, L. Ristroph, X. Zhong, M. D. Ward, J. Zhang and M. J. Shelley, *Soft Matter*, 2016, **12**, 4584–4589.
39 D. Takagi, A. B. Braunschweig, J. Zhang and M. J. Shelley, *Phys. Rev. Lett.*, 2013, **110**, 038301.
40 D. Takagi, J. Palacci, A. B. Braunschweig, M. J. Shelley and J. Zhang, *Soft Matter*, 2014, **10**, 1784–1789.
41 A. Brown and W. Poon, *Soft Matter*, 2014, **10**, 4016–4027.
42 S. Ebbens, D. A. Gregory, G. Dunderdale, J. R. Howse, Y. Ibrahim, T. B. Liverpool and R. Golestanian, *Europhys. Lett.*, 2014, **106**, 58003.
43 F. Ginot, I. Theurkauff, D. Levis, C. Ybert, L. Bocquet, L. Berthier and C. Cottin-Bizonne, *Phys. Rev. X*, 2015, **5**, 011004.
44 T. H. Besseling, M. Hermes, A. Kuijk, B. de Nijs, T. S. Deng, M. Dijkstra, A. Imhof and A. van Blaaderen, *J. Phys.: Condens. Matter*, 2015, **27**, 194109.
45 J. R. Howse, R. A. L. Jones, A. J. Ryan, T. Gough, R. Vafabakhsh and R. Golestanian, *Phys. Rev. Lett.*, 2007, **99**, 048102.
46 A. Baskaran and M. C. Marchetti, *Phys. Rev. Lett.*, 2008, **101**, 268101.
47 M. Doi and S. F. Edwards, *The theory of polymer dynamics*, Oxford University Press, 1988.
48 M. M. Tirado, C. L. Martínez and J. G. de la Torre, *J. Chem. Phys.*, 1984, **81**, 2047–2052.
49 H. H. Wensink and H. Löwen, *J. Phys.: Condens. Matter*, 2012, **24**, 464130.
50 M. E. Cates and J. Tailleur, *Annu. Rev. Condens. Matter Phys.*, 2015, **6**, 219–244.
51 A. Suma, G. Gonnella, D. Marenduzzo and E. Orlandini, *Europhys. Lett.*, 2014, **108**, 56004.
52 J. Tailleur and M. E. Cates, *Phys. Rev. Lett.*, 2008, **100**, 218103.
53 I. Theurkauff, C. Cottin-Bizonne, J. Palacci, C. Ybert and L. Bocquet, *Phys. Rev. Lett.*, 2012, **108**, 268303.
54 O. Pohl and H. Stark, *Phys. Rev. Lett.*, 2014, **112**, 118101.
55 B. M. Mognetti, A. Saric, S. Angioletti-Uberti, A. Cacciuto, C. Valeriani and D. Frenkel, *Phys. Rev. Lett.*, 2013, **111**, 245702.
56 G. S. Redner, A. Baskaran and M. F. Hagan, *Phys. Rev. E: Stat., Nonlinear, Soft Matter Phys.*, 2013, **88**, 012305.
57 M. E. Cates and J. Tailleur, *Europhys. Lett.*, 2013, **101**, 20010.
58 C. Tung, J. Harder, C. Valeriani and A. Cacciuto, *Soft Matter*, 2016, **12**, 555–561.
59 K. Chaudhary, J. J. Juarez, Q. Chen, S. Granick and J. A. Lewis, *Soft Matter*, 2014, **10**, 1320–1324.
60 S. Gangwal, O. J. Cayre and O. D. Velev, *Langmuir*, 2008, **24**, 13312–13320.
61 F. Smallenburg, H. R. Vutukuri, A. Imhof, A. van Blaaderen and M. Dijkstra, *J. Phys.: Condens. Matter*, 2012, **24**, 464113.
62 A. Kuijk, A. van Blaaderen and A. Imhof, *J. Am. Chem. Soc.*, 2011, **133**, 2346–2349.
63 A. Kuijk, A. Imhof, M. H. W. Verkuijlen, T. H. Besseling, E. R. H. van Eck and A. van Blaaderen, *Part. Part. Syst. Charact.*, 2014, **31**, 706–713.
64 H. R. Vutukuri, F. Smallenburg, S. Badaire, A. Imhof, M. Dijkstra and A. van Blaaderen, *Soft Matter*, 2014, **10**, 9110–9119.
65 M. E. Leunissen, H. R. Vutukuri and A. van Blaaderen, *Adv. Mater.*, 2009, **21**, 3116–3120.
66 J. C. Crocker and D. G. Grier, *J. Colloid Interface Sci.*, 1996, **179**, 298–310.